

Grouped Discrete Representation Guides Object-Centric Learning

Rongzhen Zhao, Vivienne Wang, Juho Kannala, Joni Pajarinen

Aalto University, Espoo 02150, Finland

{rongzhen.zhao, vivienne.wang, juho.kannala, joni.pajarinen}@aalto.fi

Keywords: Object-Centric Learning, Variational Autoencoder, Discrete Representation, Codebook Decomposition

Abstract: Similar to humans perceiving visual scenes as objects, Object-Centric Learning (OCL) can abstract dense images or videos into sparse object-level features. Transformer-based OCL handles complex textures well due to the decoding guidance of discrete representation, obtained by discretizing noisy features in image or video feature maps using template features from a codebook. However, treating features as minimal units overlooks their composing attributes, thus impeding model generalization; indexing features with natural numbers loses attribute-level commonalities and characteristics, thus diminishing heuristics for model convergence. We propose *Grouped Discrete Representation* (GDR) to address these issues by grouping features into attributes and indexing them with tuple numbers. In extensive experiments across different query initializations, dataset modalities, and model architectures, GDR consistently improves convergence and generalizability. Visualizations show that our method effectively captures attribute-level information in features. The source code will be available upon acceptance.

1 INTRODUCTION

Human vision cognition relies on the perceptual processing of visual scenes, wherein objects serve as foundational elements facilitating comprehension, reasoning, planning, and decision-making faculties (Palmeri and Gauthier, 2004; Bar, 2004; Cavanagh, 2011). Similarly, in artificial intelligence, object-level representation of images or videos is more versatile for visual tasks involving different modalities, compared to dense feature maps (Wu et al., 2023a; Ferraro et al., 2023). Object-Centric Learning (OCL) allows representing objects and the background in visual media as sparse feature vectors, along with corresponding segmentation masks as byproducts. Noteworthy, OCL achieves this usually by plain self-supervision of reconstructing the input.

The main types of OCL include mixture-based (Locatello et al., 2020; Kipf et al., 2022; Elsayed et al., 2022), transformer-based (Singh et al., 2022a; Singh et al., 2022b), foundation model-based (Seitzer et al., 2023; Zadaianchuk et al., 2023) and diffusion model-based (Wu et al., 2023b; Jiang et al., 2023) ones. Transformer-based OCL, as shown in Fig. 2 left, leverages query slots to aggregate dense feature maps into sparse object-level features (vectors), and challenges slots to capture as much object information as possible through a transformer decoder

to reconstruct a type of discrete representation as a classification task, rather than the input as a regression task. Guidance of the discrete representation, where noisy details in image or video feature map are eliminated, helps transformer-based OCL to process complex-textured objects in images or videos effectively. Such discrete representation is obtained firstly by a Variational Autoencoder (VAE) encoder encoding the input as continuous feature map, and then by a shared codebook replacing noisy detailed features in the continuous representation with its codes as template features. A codebook has a limited number of code vectors learned across all samples in a dataset, thereby forcing the codes to converge to more informative and generalizable representations.

However, existing transformer-based methods treat features as minimum units and entangle the composing attributes together, thus impeding model generalization. The natural number code indexes also fail to capture features' intrinsic information of attribute-level commonalities and characteristics, thus diminishing heuristics for model convergence.

As illustrated in Fig. 1, consider a dataset where objects consist of two attribute groups: color (black or white) and shape (triangle, square, or circle); suppose there are four objects in an image sample, for example, black-triangle, white-circle, white-square, and black-square; assume each object is downsam-

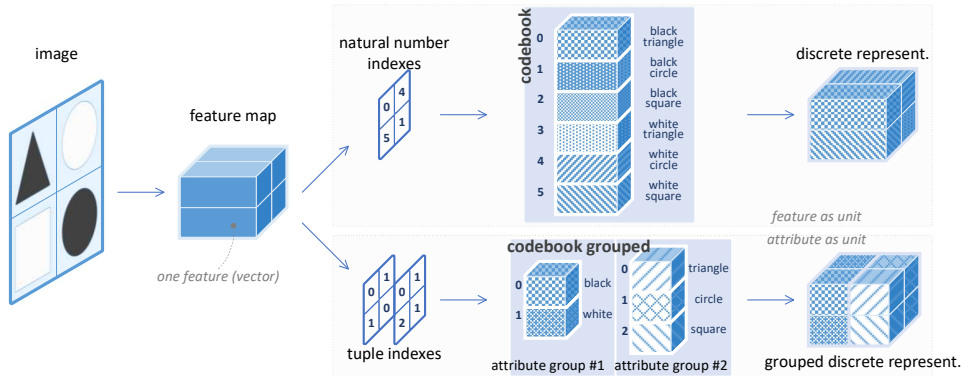


Figure 1: Representation discretization: non-grouped vs grouped. (*upper*) Existing methods take features as units and use natural number indexes to select template features from a codebook. (*lower*) We take attributes as units and use tuple indexes to select attributes from the grouped codebook and combine them into features, to facilitate OCL convergence and generalization.

pled into a feature vector in the feature map.

With the existing natural number indexing, six code indexes are needed to select template features from a codebook, i.e., natural numbers 0~5 referring to black-triangle, black-circle, black-square, and so on; then the feature map can be discretized as $\begin{bmatrix} 0 & 4 \\ 5 & 1 \end{bmatrix}$. As the codes are learnt from scratch, *the indexes hold no meaning initially and provide little guiding signal for OCL*. Suppose data are evenly distributed, then *each code vector is reused with probability $\frac{1}{6}$* .

Using our method, the codebook is decomposed into two attribute groups, and features in the feature map are discretized as combinations of template attributes selected from these two groups, i.e., $\begin{bmatrix} 0,0 & 1,1 \\ 1,2 & 0,1 \end{bmatrix}$. Here identical first/second numbers in these tuples indicate that the objects have the same attribute of color/shape, and vice versa. *This provides strong learning signals for OCL, enhancing model convergence*. Moreover, each attribute group contains fewer possible values, thus *each code is reused more with probabilities $\frac{1}{2}$ and $\frac{1}{3}$* , respectively, hopefully improves model generalizability.

In short, our contributions are as follows: (*i*) We propose *Grouped Discrete Representation (GDR)* to improve existing transformer-based OCL in both convergence and generalizability; (*ii*) We evaluate GDR’s effectiveness via extensive experiments across different dataset modalities, model architectures and query initializations; (*iii*) We provide intuitive visual interpretations of how GDR captures attribute-level commonalities and characteristics.

2 RELATED WORK

Variational Autoencoder. Among various VAEs (Sohn et al., 2015; Higgins et al., 2017; Van Den Oord

et al., 2017; Razavi et al., 2019; Gregor et al., 2019), discrete VAE (dVAE) (Singh et al., 2022a) is usually employed in transformer-based OCL (Singh et al., 2022a; Singh et al., 2022b; Seitzer et al., 2023; Zadaianchuk et al., 2023; Wu et al., 2023b; Jiang et al., 2023; Wang et al., 2023), thus we focus on our method’s effects on it instead of others. In typical dVAE (Singh et al., 2022a; Singh et al., 2022b), the intermediate representation between the encoder and decoder is discretized with feature vectors as units and natural numbers as code indexes. We group the codes into attribute-level units and perform discretization with tuples as code indexes.

Feature grouping. Grouping for better representation learning, either directly on features or on learnable parameters, (Krizhevsky et al., 2012; Huang et al., 2018; Chen et al., 2019; Gao et al., 2019; Ma et al., 2018; Zhao et al., 2021; Zhao et al., 2022) has long been explored in Convolution Neural Networks (CNN). Such a design is introduced into OCL by SysBinder (Singh et al., 2023), which groups slots directly and uses the sub-slots to aggregate object attributes from feature map to compose the final slots. We group the intermediate representation as *combinatorial* and *reusable* template attributes, and then use the grouped discrete representation to guide the aggregation from dense feature maps into slots.

Transformer decoding. Among various OCL solutions (Locatello et al., 2020; Kipf et al., 2022; Elsayed et al., 2022; Singh et al., 2022a; Singh et al., 2022b; Seitzer et al., 2023; Zadaianchuk et al., 2023; Wu et al., 2023b; Jiang et al., 2023), we focus on the ones based on transformer decoding, or transformer-based OCL. They utilize dVAE discrete representation to guide OCL of complex-textured objects. SLATE (Singh et al., 2022a) and STEVE (Singh et al., 2022b) are representatives for image and video OCL respectively. Using extra encoding as the fea-

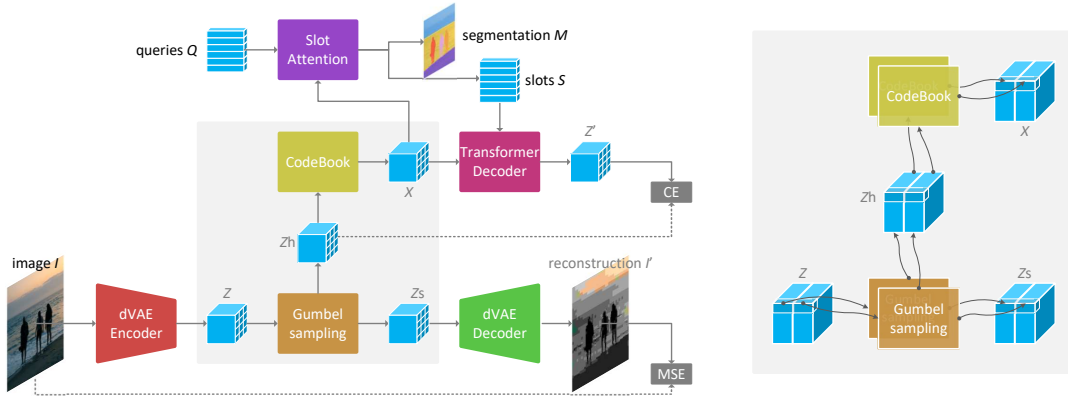


Figure 2: Discrete representation grouping in transformer-based OCL. (left) Most transformer-based OCL can be simplified into this naive architecture, where the shaded area is the original representation discretization, which takes an image as input and outputs slots and object segmentation masks. (right) Our grouped discrete representation is obtained by grouping the intermediate feature maps along the feature/channel dimension, and then doing Gumbel sampling and codebook indexing for each group as before. All the notations here are defined in Sect. 3.1.

ture map to be aggregated into slots (Jia et al., 2023; Wu et al., 2023a), rather than dVAE intermediate representation, yields SLATE⁺ and STEVE⁺. Our GDR is built upon these methods and boosts them.

Query initialization. The initial value and number of query determines the subsequent feature map aggregation into slots. As the initial scheme of shared Gaussian initialization (Locatello et al., 2020; Li et al., 2020) was proven to be too noisy (Kipf et al., 2022; Elsayed et al., 2022), non-shared random initialization (Jia et al., 2023; Chang et al., 2022) and condition initialization Then, schemes involving condition initialization (Kipf et al., 2022; Elsayed et al., 2022) (requiring extra annotation) were proposed. Some (Qian et al., 2023) argues that different samplings of the same Gaussian correspond to different instances and different Gaussians correspond to different classes. We evaluate GDR on non-shared Gaussian and condition query initialization.

3 PROPOSED METHOD

We propose *Grouped Discrete Representation* (GDR), a general technique to improve transformer-based OCL (Singh et al., 2022a; Singh et al., 2022b) in convergence and generalizability.

3.1 Discrete Representation

Most transformer-based OCL models can be simplified into the naive architecture of SLATE drawn in Fig. 2. Based on it, STEVE employs a stack of transformer encoder blocks as a recurrent module to convert current time step slots into next time step queries;

SLATE⁺ employs an extra encoder for better feature map as input to Slot Attention; STEVE⁺ employs both the recurrent module and extra encoder. Our method is a general enhancement to them, so we take SLATE to exemplify how to make the changes.

The dVAE encoder of SLATE, essentially a CNN with small spatial down-sampling, takes an image I as input and outputs logits Z

$$Z = \text{Encoder}_{\text{dVAE}}(I) \quad (1)$$

Both soft and hard Gumbel sampling (Jang et al., 2016) are applied to Z

$$Z_s = \text{softmax}\left(\frac{Z+G}{\tau}\right) \quad (2)$$

$$Z_h = \text{argmax}\left(\frac{Z+G}{\tau}\right) \quad (3)$$

where noise $G \sim \text{Gumbel}(\mu = 0, \beta = 1)$; and temperature τ schedules from 1 to 0.1 by cosine annealing during training and fixed to 0.1 during testing.

* *1st place to change.* Here each feature vector in Z is sampled as a whole into a natural number index in Z_h . We propose to sample in multiple attribute groups, as formulated in Eq. 12 and 13.

The dVAE decoder, which is a CNN with inverse up-sampling, decodes the soft sampling Z_s to reconstruct the input

$$I' = \text{Decoder}_{\text{dVAE}}(Z_s) \quad (4)$$

With the hard sampling Z_h as natural number indices, discrete representation is formed by picking template features from a codebook

$$X = \text{Codebook}(Z_h) \quad (5)$$

where Codebook is a limited-sized set of learnable code vectors, shared across all samples.

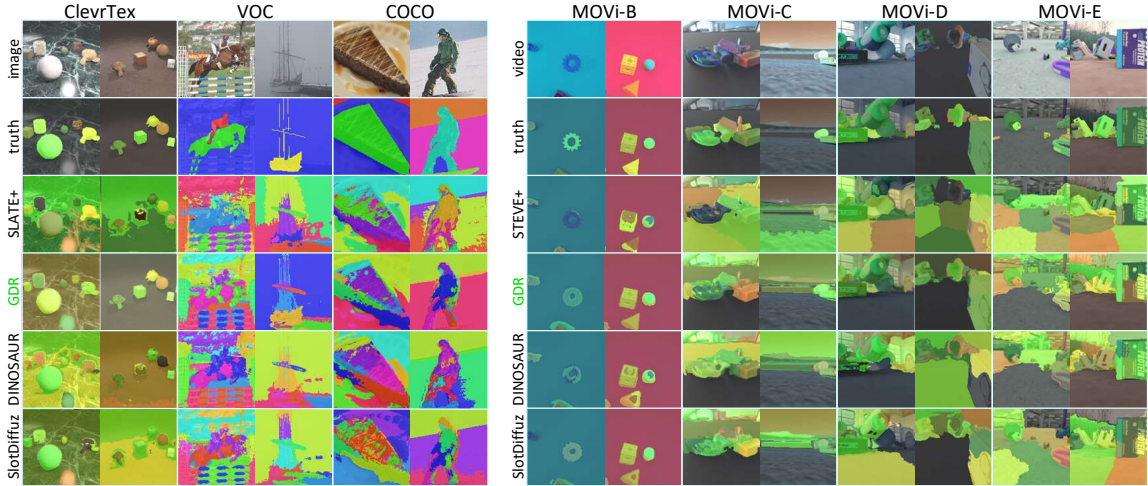


Figure 3: Visualization of unsupervised segmentation. Left is OCL with random query on images, and right is OCL with condition query on videos. The best GDR results of settings $g2$, $g4$ and $g8$ are presented here.

* 2nd place to change. Here features are taken as units, which entangles the composing attributes; and natural numbers are used as indexes, which loses features' attribute-level commonalities and characteristics. We propose to use tuple indexing and grouped codebook, as formulated in Eq. 14.

The SlotAttention (Locatello et al., 2020) aggregates the intermediate representation X into slots S with Q as query

$$S, M = \text{SlotAttention}(Q, X) \quad (6)$$

where Q is either learned Gaussian samplings or projected prior information (e.g., bounding boxes); each feature vector in slots S represents an object or background in the image; the byproduct, objects and background segmentation in the image, is obtained via argmax of attention map M along the slots.

The beginning-of-sentence (BOS) token (Jurish and Wurzner, 2013) is prepended to intermediate representation X for transformer-based decoding

$$X' = x_{\text{BOS}} \parallel X[: -1] \quad (7)$$

where \parallel means concatenation along feature vector dimension, and $[: -1]$ means dropping the last feature.

The modified intermediate discrete representation X' is decoded by a transformer decoder into logit Y , and read out by classifying every feature vector in Y as a natural number index in Z_h

$$Y = \text{TransformerDecoder}(X', S) \quad (8)$$

$$Z' = \text{Readout}(Y) \quad (9)$$

where TransformerDecoder is causally masked to challenge S to be informative; Readout is basically Linear plus softmax; Z' is the classification output.

The entire architecture is trained end-to-end by optimizing l' as regression (pre-training) and l_z as classification (training)

$$l_i = \mathbb{E}[\text{MSE}(I', I)] \quad (10)$$

$$l_z = \mathbb{E}[\text{CE}(Z', Z_h)] \quad (11)$$

where expectation $\mathbb{E}[\cdot]$ is along spatial dimensions.

3.2 Grouped Discrete Representation

Given a dataset, there are n possible c -dimensional discrete features that compose various objects and backgrounds. Suppose each discrete feature can be described by g attribute groups, and each attribute group has a possible attribute values, thus there are a^g possible combinations, and suppose $n = a^g$.

Then we need a codebook to represent these a^g possible discrete features, each of which is a c -dimensional template feature vector.

We propose a grouped tuple indexing scheme, as shown in Fig. 2, to realize intermediate discrete representation that preserves explicit attribute level feature.

Beforehand, let us define a grouped codebook of size $a \times g \times d$. (i) There are g sub-codebooks, each is an attribute group; (ii) There are a attribute values in each attribute group; (iii) Each of attribute value is a d -dimensional sub-code vector (template attribute) and $c = g \times d$; (iv) Any feature can be discretized by combination of g attributes, each of which comes from one of the sub-codebooks.

Afterwards, our method needs the following two changes in the two places mentioned in Sect. 3.1.

1st, perform grouped Gumbel sampling to obtain tuple indexes for subsequent template attribute pick-

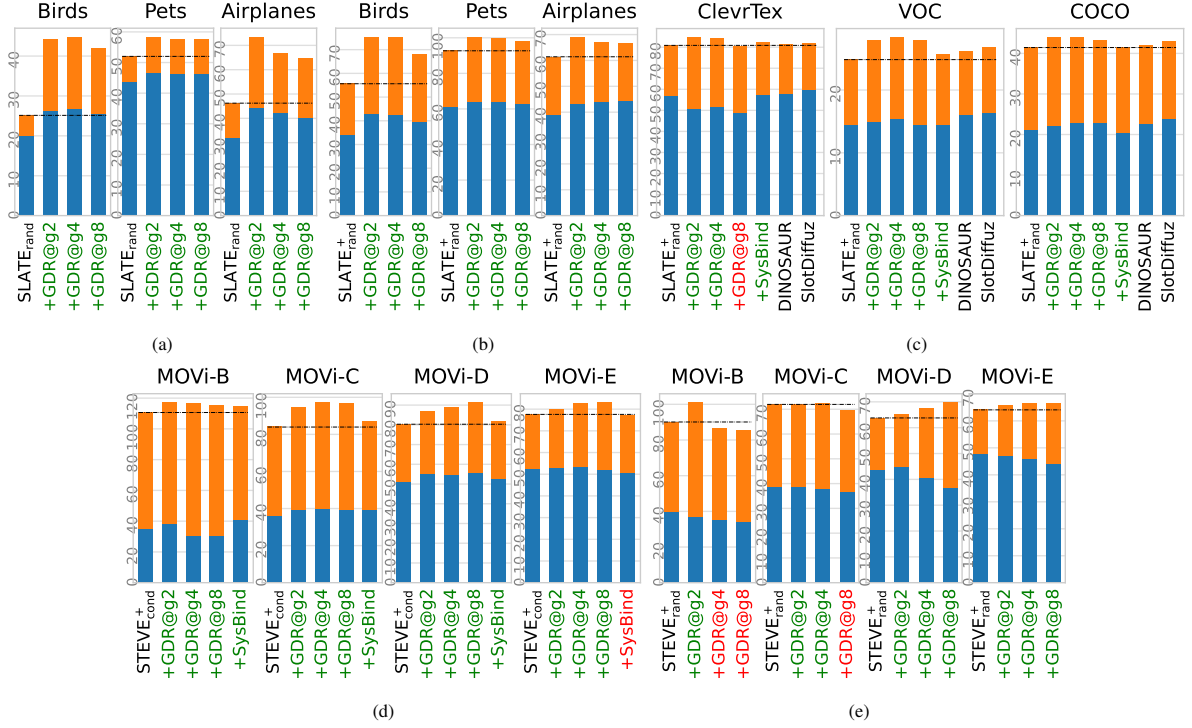


Figure 4: Unsupervised segmentation performance measured by **ARI** (all datasets) plus **IoU** (Birds, Pets and Airplanes) or **ARI** (the rest) in percent. Higher is better. (seed $\times 3$)

ing. Consequently, Eq. 2 and 3 are changed to:

$$Z_s = \text{softmax}\left(\frac{Z^1 + G^1}{\tau}\right) \parallel \text{softmax}\left(\frac{Z^2 + G^2}{\tau}\right) \parallel \dots \parallel \text{softmax}\left(\frac{Z^g + G^g}{\tau}\right) \quad (12)$$

$$Z_h = \text{argmax}\left(\frac{Z^1 + G^1}{\tau}\right) \parallel \text{argmax}\left(\frac{Z^2 + G^2}{\tau}\right) \parallel \dots \parallel \text{argmax}\left(\frac{Z^g + G^g}{\tau}\right) \quad (13)$$

where $Z^1 \dots Z^g$ are grouped from Z along the channel dimension; so do noises $G^1 \dots G^g$; \parallel denotes concatenation along the channel dimension.

2nd, select attributes from the sub-codebooks with every element in the tuple indexing as a corresponding index to form the intermediate discrete representation. Consequently, Eq. 5 is reformulated as:

$$X = \text{Codebook}_1(Z_h^1) \parallel \text{Codebook}_2(Z_h^2) \parallel \dots \parallel \text{Codebook}_g(Z_h^g) \quad (14)$$

where $Z_h^1 \dots Z_h^g$ are grouped from Z_h along channel dimension; and aforementioned codebook are grouped into sub-codebooks $\text{Codebook}_1 \dots \text{Codebook}_g$.

Note: our hard Gumbel sampling Z_h are tuple indexes, and needs to be converted back to natural number indexes for calculating the classification loss:

$$Z_h := Z_h^1 \times a^0 + Z_h^2 \times a^1 + \dots + Z_h^g \times a^{g-1} \quad (15)$$

where $Z_h^1 \dots Z_h^g$ are grouped from the original tuple Z_h along the channel dimension; and the result is the natural number Z_h .

Last, a mild loss to encourage code utilization is needed after grouping

$$l_u = -\text{entropy}(\mathbb{E}[Z_h^1]) - \text{entropy}(\mathbb{E}[Z_h^2]) - \dots - \text{entropy}(\mathbb{E}[Z_h^g]) \quad (16)$$

where $\mathbb{E}[\cdot]$ is along spatial dimensions while $\text{entropy}(\cdot)$ along the channel.

3.3 Grouped vs Non-Grouped

We compare GDR with the non-grouped solution.

Indexing schemes. (i) Although the codebook is learnt from scratch, our grouped tuple indexing offers insightful heuristics about attribute-level similarities and differences among features in the intermediate representation, leading to better *convergence*. (ii) The naive natural number indexing scheme in existing methods eliminates such semantic information, hindering effective heuristics for OCL model training.

Minimum units. (iii) With attribute-level decomposition, attributes are shared among all features as more reusable units. This allows for the construction of features through combinations of these attributes, potentially leading to *combinatorial generalization*.

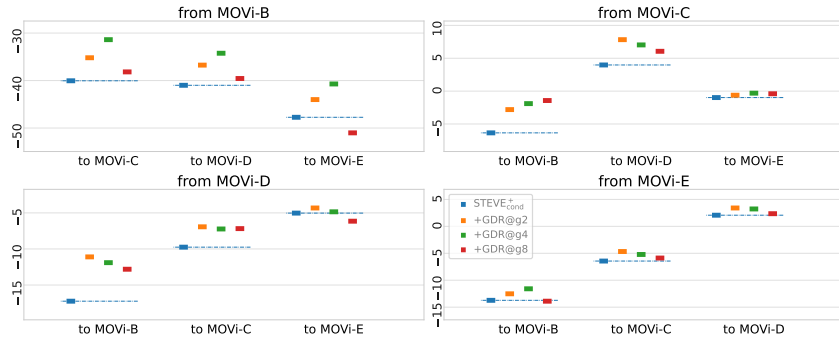


Figure 5: Zero-shot transferred segmentation performance measured by $\Delta(\text{ARI}+\text{ARI}_{\text{fg}})$ in percent, the performance drop from source to target datasets. Higher is better. (seed \times 3)

(iv) Conversely, the existing natural number indexing entangles attributes in features, which impedes the learning of generalizable attribute-level representations, especially when attributes are not uniformly distributed across datasets.

Codebook parameters. (v) Compared with the non-grouped, the available number of parameters in our grouped codebook is significantly reduced to $\frac{agd}{a^g c} = \frac{ac}{a^g c} = \frac{1}{a^{g-1}}$, e.g., only $\frac{1}{64}$ when $a = 64$, $g = 2$, $c = 256$ and $a^g = 4096$. (vi) Thus we increase c to $8c$ and use a normalization plus linear to project it back to c , resulting in $\frac{1}{1.6}$ the number of codebook parameters, still 30% less than the baselines.

Extra computation. (vii) Non-grouped computation only involves code matching using inner product for each continuous feature: $c \times n \times 1 = 256 \times 4096 = 2^{20}$; (viii) GDR computation involves code projection and matching: $((8c \times c) \times \sqrt[n]{n} \times 1) \times g$, which is 2^{26} for $g2$ and 2^{25} for $g4$. But this is negligible considering other parts of the VAE and OCL model.

4 EXPERIMENTS

We conduct comprehensive experiments to address the following questions: (i) Can GDR improve transformer-based OCL performance across different dataset modalities, model architectures and query initializations? (ii) Can GDR improve transformer-based OCL performance under zero-shot transfer among a series of datasets? (iii) What attribute information can GDR capture for object representation?

4.1 Experiment Overview

Models that are representatives of transformer-based OCL are included, with SLATE⁺ (Singh et al., 2022a) and STEVE⁺ (Singh et al., 2022b) covering *architectures* for images and videos, with SLATE (Singh

et al., 2022a) and SLATE⁺ (Jia et al., 2023) covering *implementations* of weak and strong baselines. Random (Locatello et al., 2020) and condition (Kipf et al., 2022) query *initializations* on STEVE⁺ are also covered. We include another transformer-based improver SysBinder (Singh et al., 2023), foundation-based DINOSAUR (Seitzer et al., 2023) and diffusion-based SlotDiffusion (Wu et al., 2023b) as references, skipping the outdated SlotAttention (Locatello et al., 2020) and SAVi (Kipf et al., 2022). For **fairness**, VAE encoder, decoder and codebook of all models follow that of SLATE (Singh et al., 2022a); the extra encoder follows SAVi (Kipf et al., 2022); the slot aggregation follows BO-QSA (Jia et al., 2023); the temporal predictor follows SAVi (Kipf et al., 2022); and the other parts remain the original setting.

Datasets covering cases of single/multiple *number of objects*, cases of real-world/synthetic *sources*, and cases of image/video *modalities* are included. Birds¹, Pets² and Airplanes³ are single-object real-world images; COCO⁴ and VOC⁵ are multi-object real-world images; ClevrTex⁶ are multi-object synthetic images, with confusing textures; MOVI-B/C/D/E⁷ are multi-object synthetic videos, with incremental difficulties of textures, illumination, moving views, motion blurs and so on. The data precessing follows that of SlotDiffusion (Wu et al., 2023b).

Metrics that are widely used in unsupervised segmentation evaluation are adopted, including Adjusted Rand Index (ARI)⁸, ARI of foreground (ARI_{fg}) and

¹https://www.vision.caltech.edu/datasets/cub_200_2011

²<https://www.robots.ox.ac.uk/~vgg/data/pets>

³<https://www.robots.ox.ac.uk/~vgg/data/bicos>

⁴<https://cocodataset.org/#panoptic-2020>

⁵<http://host.robots.ox.ac.uk/pascal/VOC/voc2012/index.html>

⁶<https://www.robots.ox.ac.uk/~vgg/data/clevrtex>

⁷<https://github.com/google-research/kubric/blob/main/challenges/movi>

⁸https://scikit-learn.org/stable/modules/generated/sklearn.metrics.adjusted_rand_score

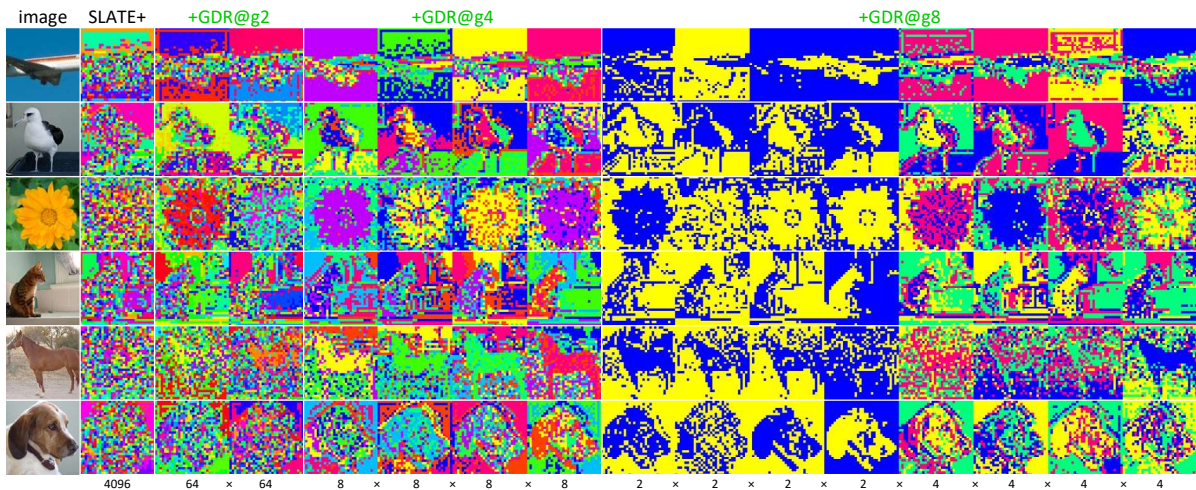


Figure 6: Visualization of code indexes of attributes in the discrete representation. Code indexes are mapped to the HSV space. Thereby, the baselines’ non-grouped indexes are visualized as single images and our GDR indexes are visualized as g images. The bottom numbers are the grouping settings, i.e., 4096 means no grouping for the baseline, (64, 64) for $g2$, (8, 8, 8, 8) for $g4$ and (2, 2, 2, 2, 4, 4, 4, 4) for $g8$, where each number limits how many possible indexes/colors are available in each column.

Intersection-over-Union of foreground (IoU)⁹. Note: (i) ARI measures the overall segmentation accuracy, but is dominated by the background, which typically has the largest area; (ii) ARI_{fg} only cares foreground objects; (iii) For single object scenes, IoU is better as ARI_{fg} may produce anomalous values. Thus, considering their similar definitions, we use $ARI+ARI_{fg}$ and $ARI+IoU$ as the overall metrics for multi- and single-object datasets, respectively.

Hyperparameters. The number of template features in the codebook is $n = a^s = 4096$. The GDR hyper-parameter g is set to 2, 4 and 8, denoted as $GDR@g2$, $g4$ and $g8$ respectively. The size of attribute groups can be determined accordingly as formulated in Sect. 3.2, i.e., (64, 64), (8, 8, 8, 8) and (2, 2, 2, 2, 4, 4, 4, 4), to make 4096 codes.

4.2 Convergence

SLATE and SLATE⁺, plus improvers GDR and SysBinder, are evaluated on Birds, Pets, Airplanes, ClevrTex, VOC and COCO, with random query initialization. STEVE⁺ and our GDR variants are evaluated on MOVi-B/C/D/E, with both condition and random query initialization. DINOSAUR and SlotDiffusion are evaluated on image datasets ClevrTex, VOC and COCO, with random query initialization.

Results in Fig. 3 and 4 demonstrate that our GDR mostly improves transformer-based OCL, making them even as good as the advanced foundation-

based and diffusion-based ones. (i) As shown in Fig. 4 *a* and *b*, GDR shows more effectiveness on weak model implementations, up to 30% of improvement, than on the strong. (ii) Comparing Fig. 4 *c* and *e*, GDR contributes more improvements to image OCL than to video OCL, with random query. (iii) According to Fig. 4 *d* and *e*, GDR works better with condition query than random query on video OCL. (iv) Compared with other methods, as shown in Fig. 4 *c*, *d* and *e*, our GDR improves the background more than the foreground. (v) For g value, single-object image OCL prefers $g2$ as in Fig. 4 *a* and *b* while multi-object image OCL prefers $g4$ as in Fig. 4 *c*. (vi) As shown in Fig. 4 *d* and *e*, $g8$ can be the best choice with condition query and on videos, but not in other cases.

Generally, we recommend using $g2$ for single-object datasets and $g4$ for multi-object datasets.

4.3 Generalizability

The models of STEVE⁺ with condition query mentioned in Sect. 4.2 are reused to evaluate zero-shot generalization among datasets MOVi-B/C/D/E. As these datasets have a varied number of objects in samples, the condition query initialization can handle this smoothly with object initial bounding boxes as query prior. And the dataset series have different scenes but with not thoroughly different objects, making them ideal for zero-shot generalization evaluation.

Results in Fig. 5 demonstrate that GDR mostly improves transformer-based OCL in generalizability under zero-shot transfer. (i) GDR of $g2$ and $g4$ always

⁹https://scikit-learn.org/stable/modules/generated/sklearn.metrics.jaccard_score.html



Figure 7: Visualization of decoded images from modified code indexes / attributes. The original image is at center, and the left and right are decoded images from the modification of the first and second attribute group of the two groups (g_2) respectively. We randomly select a segmentation area and replace the corresponding code indexes in one of the groups with a random value selected from the 64 possible code values, and decode it. Roughly, the first group learns color while the second learns texture.

shows less performance drop when the transformer-based OCL models transfer from the source dataset to the target dataset. (ii) GDR of g_8 is relatively less beneficial, and on some datasets even produces more performance drop compared with the baselines.

4.4 Interpretability

Codebook indexes being used to form the discrete representation allows visualizing the feature map by mapping these indexes to different colors in the HSV (Hue-Saturation-Value) color space. As for our grouped version, this can be done in similar ways and we get g HSV images. As shown in Fig. 6, grouping features into attributes, i.e., from non-grouped to g_2 , 4 and 8, enhances the ability of the discrete representation to distinguish among objects and the background. This suggests a stronger guidance in optimizing OCL models. However, more intuitive discrete pattern does not guarantee better OCL performance, as discussed above. Further investigation is needed.

Code indexes of the discrete representation can be further decoded by the dVAE decoder into an image. We can change one group of code indexes belonging to some object and decode it, to see what attributes of that object are changed. Results are shown in Fig. 7, taking g_2 as an example. The two attribute groups roughly learn attributes of color and texture—After replacing all the first group of code indexes, the corresponding objects or background in decoded images have different colors but the same texture, while the modification for the second group loses the texture. This shows that GDR captures attribute-level infor-

mation of those intermediate discrete features.

4.5 Ablation

How the designs in GDR affect OCL performance is illustrated by ablative experiments shown in Fig. 8.

Number of groups g in discrete representation: As discussed in Sect. 4.2 and 4.3, g_2 is suitable for simple datasets, g_4 is roughly the best in practice, and g_8 can score the highest but is unstable.

Template feature dimension in the codebook: Values of $1c$, $2c$, $4c$ and $8c$ are tested, as shown in Fig. 8 *a* the lines. Larger template feature dimension yields better OCL performance, but it saturates near $8c$.

Layer normalization (LN) in the codebook: As shown in Fig. 8 *a* the diamonds and crosses in the last column, LN is beneficial to the OCL performance, yet not that significant.

The code utilization loss l_u : The code utilization is the frequency of all possible template features being used in representation discretization, as shown in Fig. 8 *b* the curves (smoothed by Gaussian kernel¹⁰ of $\sigma = 50$). Without it, many GDR codes are never used, while the original SLATE use all codes evenly; With it, GDR code utilization improves greatly.

5 CONCLUSION

We propose to decompose features into attributes by empirically grouping template feature vectors in the

¹⁰https://docs.scipy.org/doc/scipy/reference/generated/scipy.ndimage.gaussian_filter1d.html

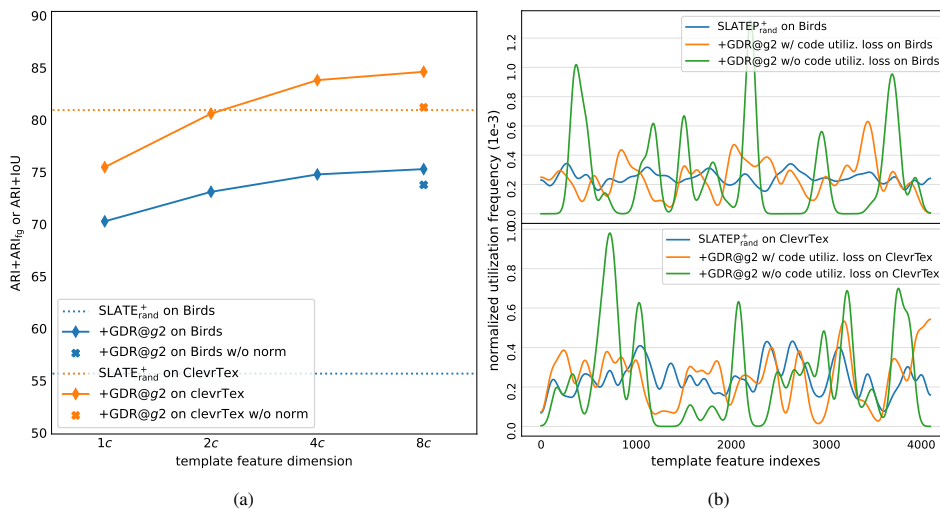


Figure 8: Ablation studies. (a) (seed $\times 5$) Lines show the effects of different template feature dimensions: 1c, 2c, 4c and 8c; Crosses and diamonds in the last column show the effects of layer “norm”alization in the codebook: with vs without. (b) Curves show the effects of the code utilization loss: with vs without.

codebook into multiple attribute sets. This technique improves the existing transformer-based OCL methods in both convergence and generalizability. Our method also shows interesting and intuitive interpretability in terms of attribute-level discrete representation patterns. Our method mainly modifies the VAE part of current transformer-based OCL models, suggesting broader applicability to other computer vision algorithm involving a VAE module.

REFERENCES

- Bar, M. (2004). Visual Objects in Context. *Nature Reviews Neuroscience*, 5(8):617–629.
- Cavanagh, P. (2011). Visual Cognition. *Vision Research*, 51(13):1538–1551.
- Chang, M., Griffiths, T., and Levine, S. (2022). Object Representations as Fixed Points: Training Iterative Refinement Algorithms with Implicit Differentiation. *NeurIPS*.
- Chen, Y., Fan, H., Xu, B., et al. (2019). Drop an Octave: Reducing Spatial Redundancy in Convolutional Neural Networks with Octave Convolution. *CVPR*.
- Elsayed, G., Mahendran, A., van Steenkiste, S., Greff, K., Mozer, M. C., and Kipf, T. (2022). SAVi++: Towards End-to-End Object-Centric Learning from Real-World Videos. *NeurIPS*.
- Ferraro, S., Mazzaglia, P., Verbelen, T., and Dhoedt, B. (2023). Focus: Object-Centric World Models for Robotics Manipulation. *NeurIPS IMOL*.
- Gao, S.-H., Cheng, M.-M., Zhao, K., Zhang, X.-Y., Yang, M.-H., and Torr, P. (2019). Res2Net: A New Multi-Scale Backbone Architecture. *TPAMI*, 43(2):652–662.
- Gregor, K., Papamakarios, G., Besse, F., Buesing, L., and Weber, T. (2019). Temporal Difference Variational Auto-Encoder. *ICLR*.
- Higgins, I., Matthey, L., Pal, A., Burgess, C. P., Glorot, X., Botvinick, M. M., Mohamed, S., and Lerchner, A. (2017). beta-VAE: Learning Basic Visual Concepts With a Constrained Variational Framework. *ICLR*.
- Huang, G., Liu, S., Van der Maaten, L., and Weinberger, K. Q. (2018). CondenseNet: An Efficient DenseNet Using Learned Group Convolutions. *CVPR*.
- Jang, E., Gu, S., and Poole, B. (2016). Categorical Reparameterization With Gumbel-Softmax. *ICLR*.
- Jia, B., Liu, Y., and Huang, S. (2023). Improving Object-Centric Learning With Query Optimization. *ICLR*.
- Jiang, J., Deng, F., Singh, G., and Ahn, S. (2023). Object-Centric Slot Diffusion. *NeurIPS*.
- Jurish, B. and Wurzner, K.-M. (2013). Word and Sentence Tokenization with Hidden Markov Models. *Journal for Language Technology and Computational Linguistics*, 28(2):61–83.
- Kipf, T., Elsayed, G. F., Mahendran, A., Stone, A., Sabour, S., Heigold, G., Jonschkowski, R., Dosovitskiy, A., and Greff, K. (2022). Conditional Object-Centric Learning from Video. *ICLR*.
- Krizhevsky, A., Sutskever, I., and Hinton, G. E. (2012). ImageNet Classification with Deep Convolutional Neural Networks. *NeurIPS*.
- Li, N., Eastwood, C., and Fisher, R. (2020). Learning Object-Centric Representations of Multi-Object Scenes from Multiple Views. *NeurIPS*.
- Locatello, F., Weissenborn, D., Unterthiner, T., Mahendran, A., Heigold, G., Uszkoreit, J., Dosovitskiy, A., and Kipf, T. (2020). Object-Centric Learning with Slot Attention. *NeurIPS*.
- Ma, N., Zhang, X., Zheng, H.-T., and Sun, J. (2018). ShuffleNet V2: Practical Guidelines for Efficient CNN Architecture Design. *ECCV*.

- Palmeri, T. J. and Gauthier, I. (2004). Visual Object Understanding. *Nature Reviews Neuroscience*, 5(4):291–303.
- Qian, R., Ding, S., Liu, X., and Lin, D. (2023). Semantics Meets Temporal Correspondence: Self-Supervised Object-Centric Learning in Videos. *ICCV*.
- Razavi, A., Van den Oord, A., and Vinyals, O. (2019). Generating Diverse High-Fidelity Images With VQ-VAE-2. *NeurIPS*.
- Seitzer, M., Horn, M., Zadaianchuk, A., et al. (2023). Bridging the Gap To Real-World Object-Centric Learning. *ICLR*.
- Singh, G., Deng, F., and Ahn, S. (2022a). Illiterate DALL-E Learns to Compose. *ICLR*.
- Singh, G., Kim, Y., and Ahn, S. (2023). Neural Systematic Binder. *ICLR*.
- Singh, G., Wu, Y.-F., and Ahn, S. (2022b). Simple Unsupervised Object-Centric Learning for Complex and Naturalistic Videos. *NeurIPS*.
- Sohn, K., Lee, H., and Yan, X. (2015). Learning Structured Output Representation Using Deep Conditional Generative Models. *NeurIPS*.
- Van Den Oord, A., Vinyals, O., et al. (2017). Neural Discrete Representation Learning. *NeurIPS*.
- Wang, Z., Shou, M. Z., and Zhang, M. (2023). Object-Centric Learning with Cyclic Walks Between Parts and Whole. *NeurIPS*.
- Wu, Z., Dvornik, N., Greff, K., Kipf, T., and Garg, A. (2023a). Slotformer: Unsupervised Visual Dynamics Simulation with Object-Centric Models. *ICLR*.
- Wu, Z., Hu, J., Lu, W., Gilitschenski, I., and Garg, A. (2023b). SlotDiffusion: Object-Centric Generative Modeling With Diffusion Models. *NeurIPS*.
- Zadaianchuk, A., Seitzer, M., and Martius, G. (2023). Object-Centric Learning for Real-World Videos by Predicting Temporal Feature Similarities. *NeurIPS*.
- Zhao, R., Li, J., and Wu, Z. (2022). Convolution of Convolution: Let Kernels Spatially Collaborate. *CVPR*.
- Zhao, R., Wu, Z., and Zhang, Q. (2021). Learnable Heterogeneous Convolution: Learning Both Topology and Strength. *Neural Networks*, 141:270–280.

APPENDIX

Here we provide the technical details.

Global Hyper-Parameters

Here are global hyper-parameters that affect the modelling, dataset and learning of all experiment items.

Input resolution of the image or video frame of all datasets `resolut0` is 128×128 .

Maximum number of slots to pre-define `num_slot`. For different datasets, we count how many objects are there in each image or video sample, and set `num_slot` to the maximum number of

objects plus the one background, instead of a global maximum number. (1) Birds, Flowers and Pets: $1 + 1$; (2) ClevrTex: $10 + 1$; (3) MOVi-B/C: $10 + 1$; (4) MOVi-D: $20 + 1$; (5) MOVi-E: $23 + 1$.

dVAE encoder output resolution `resolut1` is 32×32 , i.e., with typical spatial down sampling $4 \times$.

If there is, output resolution of the extra encoder `resolut2` is 128×128 , namely, typically with no spatial downsampling. This is specifically for SLATE⁺ and STEVE⁺ architectures.

Codebook size `num_code` is 4096.

Channel dimension of intermediate features c is 256. That is, the dimension of template features in the baseline codebook is $c = 256$.

Number of attribute sets is that we empirically group the intermediate features into g : (1) For $g = 2$, split the code indexing into a 2-tuple, whose one-hot indexes are of dimensions `groups`=[64, 64] respectively, i.e., $64 \times 64 == \text{num_code}$; (2) For $g4$, `groups`=[8, 8, 8, 8]; (3) For $g8$, [2, 2, 2, 2, 4, 4, 4, 4]. (4) Denote $g1$ as the non-grouped case, and its one-hot indexes are of dimensions [4096].

For our GDR (grouped discrete representation), we increase the intermediate feature dimension from c to $8c = 256 \times 8 = 2048$ and then projected back to c using a layer normalization and linear layer so that the total number of our codebook parameters (plus the extra layers we add) is scaled to that of the baselines level – still 1/3 less but quite enough.

Modelling Details

Transformer-Based OCL Modelling

The naive version of Transformer-base OCL models, e.g., SLATE and STEVE, is composed of: (1) A dVAE to extract intermediate representation from images or videos frames; (2) An query initializer to initialize query for slots, which supports either random sampling or priors projection; (3) The Slot Attention to aggregate the dense intermediate representation into slots by the query; (4) A Transformer decoder to challenge the slots to reconstruct the input image or frame with the help of the intermediate representation. (5) For STEVE, there is also a recurrent module, typically a Transformer encoder block, to transform current slots into next query.

The strong baseline version of Transformer-based OCL models, e.g., SLATE⁺ and STEVE⁺, is slightly different. (1) dVAE: no difference; (2) Query initializer: no difference; (3) There is an extra CNN encoder to extract finer features from images or videos, which is then used as the dense representation input of Slot Attention; (4) Slot Attention: no difference; (5) Transformer decoder: no difference. (6) For

STEVE⁺, recurrent module: no difference.

All components, except dVAE and Transformer decoder, are the same in all of our experiments.

System Binder (SysBinder)

SysBinder is also an improver to the OCL methods. We follow their core part of slot-grouping, leaving the remaining parts as the unified architecture of Transformer-based OCL methods.

Diffusion/Foundation-Based OCL Modelling

For fair comparison, we do not fully adopt the original model architecture of SlotDiffusion and DINOSAUR, because they use more advanced models like pretrained vision foundation models and ResNet as building blocks of VAE and OCL encoder.

For SlotDiffusion, to keep the unification, we replace its VQ-VAE with dVAE. But dVAE can not provide pretrained codebook parameters. Thus we employ the alignment-loss to train the codebook parameters. Remember, the codebook channel size is 4 not 256, thus we need an extra project, i.e., a linear layer, to project the 4096 channel size down to 4.

For DINOSAUR, their employment of DINO vision foundation model is one of the main boosts to OCL performance. We replace it with the unified CNN encoder, which is also used by other OCL models, and still follow the pretraining method of DINO original work. Decoder is the mixture-based.

dVAE

The dVAE module is learnt to represent any images or video frames in a dataset with limited number of template features picked from a codebook.

It consists of a CNN encoder, discretizer and CNN decoder, where the discretizer is formulated in the main text Eq. 2, 3 and 5. The discretizer consists of Gumbel sampling and a codebook. For the codebook, as described in the main text, we have two choices: the baseline, non-grouped codebook of size $n \times c$, where $n = 4096$ and $c = 256$; and our GDR, grouped codebook of size $a \times g \times d$, where $a^g = n$ and $d = 8c/g$. But in practice, there are non-divisible cases, then we follow rules detailed above, about how to determine `num_code`, `g`, `groups` and `g_dims`.

We identically use such CNN encoders and decoders across different OCL models and datasets.

Extra CNN Encoder

For strong baseline versions, i.e., SLATE⁺, STEVE⁺, we need an extra CNN encoder to encode the input image or video frame into feature map without spatial downsampling for better aggregation in Slot Attention later. For naive version, i.e., SLATE and STEVE, there is no such a component.

This extra encoder is a naive CNN backbone without spatial down sampling: four convolution layers of kernel size 5 stacked with ReLU activations.

This component is identically shared across all OCL models and datasets for comparison fairness.

Query Initializer

The query initializer is used to provide initial value for aggregating dense feature map into slots that represent different objects and the background.

One way to obtain such an initialization is by learning a set of Gaussian distributions and sample from them. We have parameters for mean and variance respectively. The latter is not trainable, instead, it is scheduled with cosine annealing.

Another way for initialization is projecting the prior information about objects and the background, e.g., bounding boxes, into a set of vectors: (1) Firstly, Bounding boxes are normalized by dividing them with the height and width of the input image or video frame, and then flattened into a set of 4-dimensional vector, whose number is the number of slots; (2) Afterwards, they are processed by a two-layer MLP, with GELU as the activation, to project them into the channel dimension of c , the same as the slots.

This component is identically shared across all OCL models and datasets for comparison fairness.

Slot Attention

For this part, we just use the original version of Slot Attention. This component is identically shared across all OCL models and datasets for comparison fairness, except the following two points.

For naive OCL models, SLATE and STEVE, we use intermediate feature from dVAE as the key and value. For strong baseline version of models, SLATE⁺ and STEVE⁺, we use the output feature map from the extra CNN encoder.

Here we have one hyper-parameter `num_iter`, the number of iterations for aggregating the dense feature map into the slots. (1) For random query initialization, we use `num_iter=3` as no sufficient information from initial query, multiple aggregation iterations needed; (2) For condition query initialization, we use `num_iter=1` as the prior already provide sufficient information, single aggregation iteration enough.

Transformer Decoder

This decoder takes the intermediate representation (after position embedding) as target, and takes the slots as memory. It finally outputs logits of dimension `num_code = 4096` as a classification, with the one-hot indexing of the intermediate representation as ground-truth, for reconstructing the input. To challenge the slots further, the last token in the intermediate representation is removed and a Beginning-of-Sentence token is prepended to the beginning. And along with the causal masking, the decoder tries to predict every next token in the target.

This component is identical across all OCL mod-

els and datasets for comparison fairness.

Dataset Details

Datasets are Birds, ClevrTex, Flowers, Pets, COCO, VOC, as well as MOVi-B/C/D/E.

Dataset Conversion

All datasets are converted into compressed LMDB format so as to put into the RAM disk or NVMe high throughput disk to minimize I/O overhead and maximize clusters' computation power.

Every sample is wrapped in a key-value pair package containing the following values: (i) Image or video of data type uint8, which is center-cropped and re-sampled into spatial size 128, 128; (ii) Segmentation annotation of the image or video of data type uint8, in index format rather than multi-channel format, which is accordingly center-cropped and re-sampled into spatial size 128, 128 under interpolation method of NEASET-EXACT due to the index format; (iii) Bounding boxes in this image or video frames of data type float32, which is re-calibrated to match the aforementioned center-cropping and normalized /divided by the spatial dimension 128.

Data Pre-Processing

During training, before feeding sample batches into models, it is quite unified to do the data pre-processing. (i) For every video sample, we randomly time-crop it of time window 6, which is done on video data block, segmentation masks and bounding boxes accordingly; (ii) The image or video data block in a key-value pair package is normalized between $[-1, 1]$ by minus 127.5 and dividing 127.5; (iii) For datasets with bounding boxes, we pad them to the maximum number of slots predefined above.

During evaluation, everything is the same as that of training but that we do not do the time-cropping.

Learning Details

There are two stages of training in total.

Pre-Training of dVAE Model

For all datasets, we use total number of training iterations 2,5000, and validation interval iterations 500, so that we have about 50 checkpoints for every OCL model on every dataset. The batch size for image datasets is 64, while for video datasets it is 16. For multi-process, we use the number of workers 4. This holds for both training and validation.

The objective function is the one formulated in Eq. 10, namely, the MSE loss between the reconstructed image/video and the input image/video. No metrics is needed here. Just use the objective function for model selection after pre-training. We use Adam optimizer

with initial learning rate of $2e-3$. And the learning rate is manipulated by cosine annealing scheduling, with a linear warmup during first 1250 steps.

We use auto mixed precision using PyTorch autocast. Together, we use PyTorch gradient scaler, so as to apply gradient clipping of maximum norm 1.0.

Here to balance the exploration and exploitation, we manipulate the τ value for dVAE's Gumbel sampling. It starts from 1 at training start and decays to 0.1 at end under cosine annealing scheduling. During validation or testing, this value is of course not valid as we use argmax instead of Gumbel sampling.

Training of OCL Model

For all datasets, we use total number of training iterations 5,0000, and validation interval iterations 1000, so that we have about 50 checkpoints for every OCL model on every dataset.

The batch size for image datasets is 32 for both training and validation, while for video datasets it is 8 for training and 4 for validation as there are more timesteps in videos during validation.

For multi-process, we use the number of workers 4. This holds for both training and validation.

The objective function is the one formulated in Eq. 11, namely, the CE loss between the predicted image/video token classes and the discrete intermediate representation of input image/video. Metrics used here are ARI, calculating the panoptic segmentation accuracy of both objects and the background, ARI_{fg} , calculating the instance segmentation accuracy of the foreground objects only (for multi-object datasets), and IoU, calculating the instance segmentation accuracy of the foreground object only (for single-object datasets).

We use Adam optimizer with initial learning rate of $2e-4$. And the learning rate is manipulated by cosine annealing scheduling, with a linear warmup during first 2500 steps. We use auto mixed precision provided by PyTorch `autocast` API. Along with this, we use PyTorch builtin gradient scaler, so as to apply gradient clipping of maximum norm 1.0.

For random query initialization, we manipulate the σ value of the learned non-shared Gaussian distribution to balance the exploration and exploitation. On multi-object datasets, it starts from 1 at training start and decays to 0 at training end under cosine annealing scheduling; but on single-object datasets, it remains 0 from beginning to the end. During validation or testing, this value is set to 0, eliminating any uncertainty for best performance.